PCCP

PAPER

Check for updates

Cite this: *Phys. Chem. Chem. Phys.*, 2018, **20**, 12817

Thermal decomposition of $FC(O)OCH_3$ and $FC(O)OCH_2CH_3$†

M. Berasategui, G. A. Argüello and M. A. Burgos Paci *

Received 27th December 2017,
Accepted 28th March 2018

DOI: 10.1039/c7cp08656c

rsc.li/pccp

The thermal decomposition of methyl and ethyl formates has been extensively studied due to their importance in the oxidation of several fuels, pesticidal properties and their presence in interstellar space. We hitherto present the study of the thermal decomposition of methyl and ethyl fluoroformates, which could help in the elucidation of the reaction mechanisms. The reaction mechanisms were studied using FTIR spectroscopy in the temperature range of 453–733 K in the presence of different pressures of N_2 as bath gas. For $FC(O)OCH_3$ two different channels were observed; the unimolecular decomposition which is favored at higher temperatures and has a rate constant $k_{FC(O)OCH_3} = (5.3 \pm 0.5) \times 10^{15} \exp[-(246 \pm 10\ \text{kJ mol}^{-1}/RT)]$ (in units of s^{-1}) and a bimolecular channel with a rate constant $k_{FC(O)OCH_3} = (1.6 \pm 0.5) \times 10^{11} \exp[-(148 \pm 10\ \text{kJ mol}^{-1}/RT)]$ (in units of s^{-1} (mol L)$^{-1}$). However for ethyl formate, only direct elimination of CO_2, HF and ethylene operates. The rate constants of the homogeneous first-order process fit the Arrhenius equation $k_{FC(O)OCH_2CH_3} = (2.06 \pm 0.09) \times 10^{13} \exp[-(169 \pm 6\ \text{kJ mol}^{-1}/RT)]$ (in units of s^{-1}). The difference between the mechanisms of the two fluoroformates relies on the stabilization of a six-centered transition state that only exists for ethyl formate. First principles calculations for the different channels were carried out to understand the dynamics of the decomposition.

1. Introduction

The reaction between RC(O)F and alcohols can be thought of as a potential sink for methanol or ethanol in the atmosphere following the work by Argüello *et al.* who studied the mechanism and the kinetics of FC(O)F and FC(O)OOC(O)F with methanol at different temperatures.[1,2] They proposed that the reaction may be catalyzed heterogeneously by aerosols, particulate matter, water droplets, *etc.*, giving a mean lifetime of 6 min at 25 °C for CH_3OH when the reaction was carried out on an active surface. The main products of these reactions are HF and the corresponding formate, $RC(O)OCH_3$.

Several studies on thermal decomposition of methyl formates have been performed using different techniques. In particular, $HC(O)OCH_3$, the simplest member of the ester family, is a well-known reagent used as a precursor of many organic compounds like formic and acetic acids and has been found to be a byproduct of the oxidation of several proposed fuel alternatives.[3–7] The major products of its thermal decomposition observed are methanol, carbon monoxide, and formaldehyde.[8–10] Based on these products, Steacie proposed the following mechanism [8]

$$HC(O)OCH_3 \rightarrow CH_3OH + CO \quad (1)$$

$$CH_3OH \rightarrow CH_2O + H_2 \quad (2)$$

Jain and Murwaha[9] reported that the decomposition of methyl formate does not involve free radical reactions and occurs *via* the hydroxymethylene (HCOH) intermediate according to the following reactions

$$HC(O)OCH_3 \rightarrow CH_2O + HCOH \quad (3)$$

$$HCOH \rightarrow CH_2O \quad (4)$$

Francisco[11] examined this mechanism with the *ab initio* molecular orbital theory and found, besides the channel described in (1), two new ones

$$HC(O)OCH_3 \rightarrow CH_4 + CO_2 \quad (5)$$

$$HC(O)OCH_3 \rightarrow 2CH_2O \quad (6)$$

for which their transition states were found. Based on the activation energies, the main mechanism proposed by Francisco comprises channels (1) and (6) while channel (5) may become important only at higher energies. His results agree with those of shock tube/laser absorption studies by Ren *et al.*[12]

Waddington and Ramsperger[13] studied the thermal decomposition of trichloromethyl chloroformate at temperatures between 533 and 583 K. The main product of this reaction is CCl_2O, while in the condensed phase it may produce CCl_4 and CO_2.[14,15] The reaction has been found to be first order and homogeneous. The rate constant found for the reaction $ClC(O)OCCl_3 \rightarrow 2CCl_2O$ follows

INFIQC, Departamento de Físico Química, Facultad de Ciencias Químicas, Universidad Nacional de Córdoba, Ciudad Universitaria, Córdoba X5000HUA, Argentina. E-mail: mburgos@fcq.unc.edu.ar

† Electronic supplementary information (ESI) available. See DOI: 10.1039/c7cp08656c

the expression $k_{ClC(O)OCCl_3} = 1.4 \times 10^{13} \exp[-(60.7 \text{ kJ mol}^{-1}/RT)]$ (in units of s^{-1}). Johnson *et al.*[16] studied the pyrolysis of $ClC(O)OCH_3$ in the presence of inhibitors between 698 and 753 K and found methyl chloride and carbon dioxide as products according to the following homogeneous molecular reaction

$$ClC(O)OCH_3 \rightarrow CH_3Cl + CO_2 \quad (7)$$

The rate constant is given by $k_7 = 1.4 \times 10^{(14.3\pm0.2)} \exp[-251 \pm 2 \text{ kJ mol}^{-1}/RT] \text{ s}^{-1}$ and the reaction proceeds by a four-center transition state. They also found that at temperatures above 700 K the reaction produces byproducts assigned to heterogeneous processes.

As long as we are concerned, although there are many studies on $XC(O)OCH_3$ molecules (with X = H and Cl), no studies on the thermal decomposition of $FC(O)OCH_3$ have been conducted. This molecule is the most polar of the family and its study may clarify the mechanism of pyrolysis of the $XC(O)OCH_3$ family.

On the other hand, little is known about ethyl fluoroformate, $FC(O)OCH_2CH_3$. Previous studies[17,18] reported the synthesis in the condensed phase by the use of different solvents or surface catalysis. Here we propose a new synthetic method from the direct reaction between CF_2O and ethanol in the gas phase and at room temperature to produce $FC(O)OCH_2CH_3$ and HF in high yield and purity.

In contrast, ethyl formate, $HC(O)OCH_2CH_3$, has been widely studied. It is produced naturally in a variety of products,[19,20] and it has shown insecticidal, fungicidal, larvicidal and pesticidal properties.[21–23] Due to its intrinsic advantage of being volatile, ethyl formate has been used for fumigation of commodities and for pests associated with dried fruit.[24] Besides, it has been found to be formed in the photooxidation of diethyl ether with yields between 66 and 92%.[25,26] The detection of ethyl formate in the interstellar space has also been reported by Belloche *et al.*[27] Therefore, the unimolecular reactions of ethyl formates are crucial for understanding interstellar chemistry as well as atmospheric processes. Chou studied the unimolecular decomposition of $HC(O)OCH_2CH_3$ in the S_0 state.[28,29] He proposed that this reaction may occur by a six center transition state. Blades, who confirmed Chou's six center TS, obtained an experimental rate constant expression of $k = 2.13 \times 10^{11} \exp[-184.6 \pm 0.4 \text{ kJ mol}^{-1}/RT] \text{ s}^{-1}$, with an entropy for the transition state of $-10.7 \text{ J mol}^{-1} \text{ K}^{-1}$ at 800 K,[30] which is entirely consistent with the TS proposed.

Herein we present a thorough study of the thermal decomposition of $FC(O)OCH_3$ and $FC(O)OCH_2CH_3$ at different temperatures and total pressures that were also supported by high level *ab initio* calculations in an attempt to shed light on the chemistry of the atmospheres.

2. Experimental section

2.1. Instrumentation

(a) Vibrational spectroscopy. Gas-phase infrared spectra in the range of 4500–400 cm^{-1} were recorded with a resolution of 2 cm^{-1} from 32 co-added interferograms using an FTIR instrument (Bruker IFS66V) equipped with a photoconductive MCT detector. The OPUS® software was used to analyze and manipulate the IR spectra. Due to the fast decomposition of the sample at temperatures higher than 720 K ($FC(O)OCH_3$ fully decomposes in less than 50 seconds), we used the Rapid-Scan FTIR Time-Resolved method to obtain enough spectra for kinetic analysis. In this method the mirror was moved at velocities higher than 0.1 cm s^{-1}, allowing a resolution time of only a few seconds for our experiments. Single-sided interferograms were acquired only during the forward movement of the mirror. The spectral range for these experiments was 4000–700 cm^{-1} and the spectral resolution was maintained at 2 cm^{-1}.

(b) Infrared cells. In order to minimize heterogeneous reactions when achieving the required temperatures (563–733 K), we used a stainless steel cell (optical path length 100 mm) with silicon windows, wrapped with an electrical resistor connected to an Instrelec® temperature controller (NC201-V) and isolated with ceramic fibers from the environment.

(c) Computational details. First principles calculations were carried out using DFT, with the Becke's three-parameter hybrid functional method using the Lee–Yang–Parr correlation functional (B3LYP) in combination with different basis sets. The superiority of DFT methods over conventional Hartree–Fock methods for the study of fluoro-carbon-oxygenated compounds has previously been demonstrated, and the determination of geometric parameters for this kind of systems yielded accurate results in comparison with gas electron diffraction experiments shown.[31–33] As DFT methods take into account the electron correlation energy only in part,[34] we think that the 6-31++G(d,p) and 6-311++G(3d,2p) basis sets should be adequate to describe the relative energies for the isomers. Additionally, harmonic vibrational frequencies and zero-point energies (ZPE) were calculated at the same level of theory to check whether the stationary points obtained were either isomers or first-order transition states. All calculated conformers had only real frequencies. The determination of the Hessian matrix also enabled the calculation of the thermochemical quantities for the conformers at 298.15 K.

The Møller–Plesset expansion truncated at second-order (MP2), and the high accuracy energy method Gaussian-4 (G4) was also used for the calculation of the activation energies for a more complete comparison. All symmetry restrictions were turned off in the calculations. Intrinsic Reaction Coordinate (IRC) calculations were carried out for all the transition states in order to guarantee the connection between the latter and the minima in the PES. All calculations were run with the Gaussian 09 program package.[35]

2.2. General procedures and reagents

Volatile materials were manipulated in a glass vacuum line equipped with two capacitance pressure gauges (0–760 Torr, MKS Baratron; 0–70 mbar, Bell and Howell), three U traps, and valves with poly(tetrafluoroethylene) stems (Young, London). The vacuum line was connected directly to the stainless steel IR gas cell placed in the sample compartment of the FTIR instrument. For thermal decomposition experiments, typically 5–10 mbar of the reagent ($FC(O)OCH_3$ or $FC(O)OCH_2CH_3$) was loaded into

 This journal is © the Owner Societies 2018

the reaction cell and the final pressure was reached with N_2. The experiments were repeated at different temperatures in the range of 563–733 K.

The reaction between CF_2O and $CH_3OC(O)OCH_3$ was carried out in a stainless steel thermal reactor to avoid the heterogeneous reaction of CF_2O with the silicon windows at the working temperatures (513–573 K). Small amounts (less than 5%) of the sample were added into the IR cell every 5 minutes to follow the course of the reaction. The cell and the reactor were connected by a PTFE pipe using stainless steel Swagelok's® valves and connectors to avoid secondary reactions with silicon surfaces.

Most of the products obtained (CO_2, CO, HF, HCl, *etc.*) were identified and quantified from the reference spectra of pure samples.

2.3. Chemicals

The synthesis of CF_2O was carried out by the photolysis of $(CF_3C(O))_2O$ ($\sim$50 mbar) in the presence of 150 mbar of CO and 500 mbar of O_2 (>99.9%, Air Liquide). The photoreactor consisted of a one-neck 12 L glass round-bottom flask with a 30 cm-long double-walled water-jacketed quartz tube inside, in which a 40 W low-pressure mercury lamp (Heraeus, Hanau) was placed. The sample was purified by fractional distillation at low temperatures until $\sim$99% of CF_2O was obtained.[1]

$FC(O)OCH_2CH_3$ and $FC(O)OCH_3$ samples were synthesized from the reaction between CH_3CH_2OH ($\geq$99.5%, Dorwil) and CH_3OH (99.9%, OPTIMA-Fisher), respectively, with excess of CF_2O at room temperature. The reactor used consisted of a one-neck 12 L glass round-bottom flask. After evacuation of the reactor, the inner surface was conditioned with CF_2O (100 mbar) for a couple of hours to remove residual water from the surface. The reactor was loaded with partial pressures of 40.0 mbar for CF_2O and 20.0 mbar for the alcohol (CH_3OH and CH_3CH_2OH). The excess of CF_2O prevented the formation of $CH_3OC(O)OCH_3$ or $CH_3CH_2OC(O)OCH_2CH_3$ respectively. Every 15 min, a small amount of the gas mixture (0.8% of the reactor content) was analyzed by IR spectroscopy. In particular, the bands at 1947 (CF_2O), 1055 (CH_3OH), and 1066 cm^{-1} (CH_3CH_2OH) were suitable for monitoring their disappearance. The reaction was stopped when the band of the alcohol had disappeared (about 1 h in both cases). The contents of several batches were collected by slowly passing the content of the reactor through three U traps kept at −196 °C. To purify the collected raw products, they were kept at −80 °C and small batches were pumped out. In this manner, the more volatile compounds (CF_2O and HF) were first monitored by their IR bands (1947 cm^{-1} for CF_2O, and $\sim$4000 cm^{-1} for HF) and then discarded. The pre-purified sample was afterward repeatedly splitted through three U traps held at −40, −80, and −120 °C in dynamic vacuum until almost pure (>99,5%) FC(O)OR was obtained. The overall yield was >98% with respect to the initial CF_2O.

The IR absorption cross section for some bands of the title molecules was obtained from the pressure dependence of the absorbance. For the band at 1860 cm^{-1} of $FC(O)OCH_3$ the slope of the calibration curve was $(2.006 \pm 0.003) \times 10^{-20}$ cm^3 per molecule, with zero intercept. Considering that the infrared cell used for this measurements has a path length of 23 cm, the absorption coefficient found at room temperature was $(8.7 \pm 0.1) \times 10^{-22}$ cm^2 per molecule (int. cross section $4.75 \pm 0.5 \times 10^{-20}$ cm per molecule). For the band at 1852 cm^{-1} of $FC(O)OCH_2CH_3$ the slope of the curve was $(1.818 \pm 0.005) \times 10^{-20}$ cm^3 per molecule, so the absorption coefficient was $(7.9 \pm 0.1) \times 10^{-22}$ cm^2 per molecule (int. cross section $2.35 \pm 0.03 \times 10^{-20}$ cm per molecule).

$CH_3OC(O)OCH_3$ was obtained from commercial sources ($\geq$99%, Sigma-Aldrich) and used without further purification. N_2 (>99.9%, Linde) used as bath gas was also obtained from commercial sources.

3. Results and discussion

3.1. Thermal decomposition of $FC(O)OCH_3$

In order to determine the products of the decomposition reaction, 10.8 ± 0.1 mbar was loaded into the cell at 698 K and the sample was analyzed by IR spectroscopy at 20 s intervals. Fig. 1 shows the reagent and products of the thermal reaction after 400 seconds. It is evident that the main products found were CO_2 and CH_3F, as well as minor concentrations of $CH_3OC(O)OCH_3$, CH_3OCH_3 and SiF_4 from the comparison of the "products" trace with reference spectra used for identification, all of which are shown in the figure. Based on these products, the main channel proposed for the decomposition mechanism consists of the following concerted step

$$FC(O)OCH_3 \rightarrow CH_3F + CO_2 \quad (8)$$

Fig. 2 shows the time evolution of the concentration of $FC(O)OCH_3$, CO_2 (left scale in the figure) and the addition of both (right scale). Should reaction (8) be the only channel, without side processes, the sum of reagent and CO_2 concentrations should be constant with time; nevertheless, the evolution of this sum has a minimum around 650 s, indicating the presence of other channels. A secondary reaction path is proposed

$$2\ FC(O)OCH_3 \rightleftharpoons CH_3OC(O)OCH_3 + CF_2O \quad (9)$$

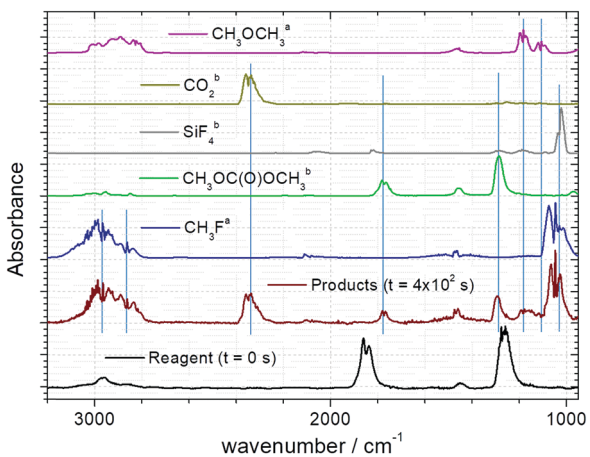

Fig. 1 Spectra comparison of the reagent ($FC(O)OCH_3$) and the products at 698 K after 400 seconds [a]from the NIST database, [b]From our own inventory.

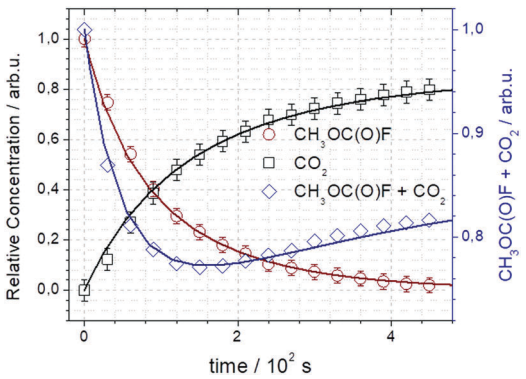

Fig. 2 Time dependence of the relative concentrations of $FC(O)OCH_3$ and CO_2. Blue diamonds correspond to the addition of both concentrations. Solid lines correspond to the kinetic simulation.

In this case, two molecules of $FC(O)OCH_3$ combine to produce $CH_3OC(O)OCH_3$ and CF_2O. Although CF_2O was not detected by IR spectroscopy, it could be reacting with the silicon windows resulting in the formation of SiF_4 and CO. Small concentrations of SiF_4 were detected in the region of 1000–1050 cm^{-1}. The formation of this product becomes evident when the IR spectrum of CH_3F is subtracted from the spectrum of the products, this is shown in Fig. S1 (ESI†). Another evidence of reaction (9) is the fact that, at lower temperatures the concentrations of SiF_4 and CO increase as CH_3F and CO_2 decrease (also showed in Fig. S1(a), ESI†). Based on these observations, it can be assumed that at temperatures lower than 660 K the predominant reaction is (9). A similar two channel mechanism has been proposed by Pepino *et al.* in the thermal decomposition of 2,Cl-ethyl isocyanate in the gas phase.[36] Even though the authors did not observe the presence of the product of the dimerization reaction – imine formation, they proposed a mechanism based on the IR results.

In order to further confirm this path, we carried out the reverse thermal reaction by mixing pure samples of $CH_3OC(O)OCH_3$ and CF_2O (Fig. S1(b), ESI†), observing the appearance of $FC(O)OCH_3$. This is an indication that reaction (9) occurs.

Finally, $CH_3OC(O)OCH_3$ may be decomposed into CH_3OCH_3 and CO_2 as Peukert *et al.* have proposed[37]

$$CH_3OC(O)OCH_3 \rightarrow CH_3OCH_3 + CO_2 \qquad (10)$$

In this manner, the anomalous increase of CO_2 after 180 seconds, as well as the appearance of CH_3OCH_3, would be explained. The complete mechanism for the thermal decomposition of $FC(O)OCH_3$ was simulated with the Kintecus program package.[38] The input parameters were the experimental rate constant of reaction (8), and the concentration of the reactant and CO_2 while the fitted rate constants obtained were $k_9 = 8.3 \pm 0.8 \times 10^{-4}$ L mol^{-1} s^{-1} and $k_{10} = 3.8 \pm 0.4 \times 10^{-3}$ s^{-1}. The solid lines in Fig. 2 correspond to the time evolution obtained from the simulation. As it can be seen, the agreement with the experimental data is excellent.

To study the thermochemical kinetic parameters involved in this process, the experiment was repeated at different temperatures between 563 and 733 K. The reaction was followed by monitoring the 1860 cm^{-1} band of $FC(O)OCH_3$. No pressure dependence of the rate constant was observed when 10 mbar of $FC(O)OCH_3$ was diluted with different pressures of N_2 to reach total pressures of 260, 392, 525 and 1000 mbar (though only experiments run at some selected pressures are plotted in Fig. 3(b)). For each temperature the reaction order for the disappearance of the reagent was evaluated using the half-life method. The relation between the initial concentration of the reagent and the half-life is given by the following equation:

$$\log(t_{1/2}) = \log\frac{2^{(n-1)} - 1}{(n-1)k_A} - (n-1)\log\left[FC(O)OCH_3\right]_0$$

where n is the reaction order and can be obtained from the slope of the plot $\log(t_{1/2})$ *vs.* $\log([FC(O)OCH_3]_0)$. This is shown for four different temperatures in column (a) of Fig. S2 (ESI†). It is observed that the reaction order tends to two for lower temperatures and to one for higher temperatures. In addition, in Fig. S2(b) (ESI†) the kinetic law for the decomposition of the unimolecular reaction is plotted ($\ln(A)$ *vs.* time) and in Fig. S2(c) (ESI†) the kinetic evolution for a bimolecular reaction is plotted ($1/A$ *vs.* time). In the first case, the linearity of the data points is reached at higher temperatures, whereas in the second case it is reached at lower temperatures. This is an indication that at lower temperatures the decomposition goes through the bimolecular reaction (9), but at higher temperatures the unimolecular channel (reaction (8)) is dominant.

To evaluate the uni- and bi-molecular rate constants at each temperature, the time evolution of the disappearance of the reagent was modeled considering reactions (8) and (9). In this model, k_8 and k_9 are the adjustable parameters to fit the experimental data points (red solid lines in Fig. S2(b) and S2(c), ESI†).

Fig. 3(a) shows the temperature dependence of the reaction order for the whole range. A sigmoidal tendency is observed and fitting was performed using the equation as shown in the figure. As the reaction is too slow at lower temperatures, the half-life method could not be performed for the three lowest points. For this reason they were obtained from the fitting (denoted in blue circles), and used to get rate constants k_8 and k_9 for each temperature.

With each pair of rate constant Arrhenius analysis was performed to obtain the activation energy and pre-exponential factor for each path. In Fig. 3(b) both Arrhenius plots are displayed, as well as the rate constant was obtained considering the reaction as a unimolecular process. From the linear fitting of k_8 the activation energy and pre-exponential factor of (246 ± 2) kJ mol^{-1} and $(5.3 \pm 0.2) \times 10^{15}$ s^{-1} were obtained and from k_9, (148 ± 1) kJ mol^{-1} and $(1.6 \pm 0.1) \times 10^{11}$ s^{-1} $(mol\ L)^{-1}$ respectively. Although these errors were taken from the deviation of the linear fitting, we consider a ~5% error to be more reliable with the experimental procedure, so the value of the E_a is (246 ± 10) kJ mol^{-1} for k_8 and (148 ± 10) kJ mol^{-1} for k_9.

Comparing the values obtained for the unimolecular decomposition (k_8) with those for the thermal decomposition of $HC(O)OCH_3$, carried out in the range of temperatures 1202–1607 K (E_a = 242 kJ mol^{-1} and $A = 4.4 \times 10^{11}$ s^{-1}),[12] it is evident that the activation energies are very similar for both molecules.

 This journal is © the Owner Societies 2018

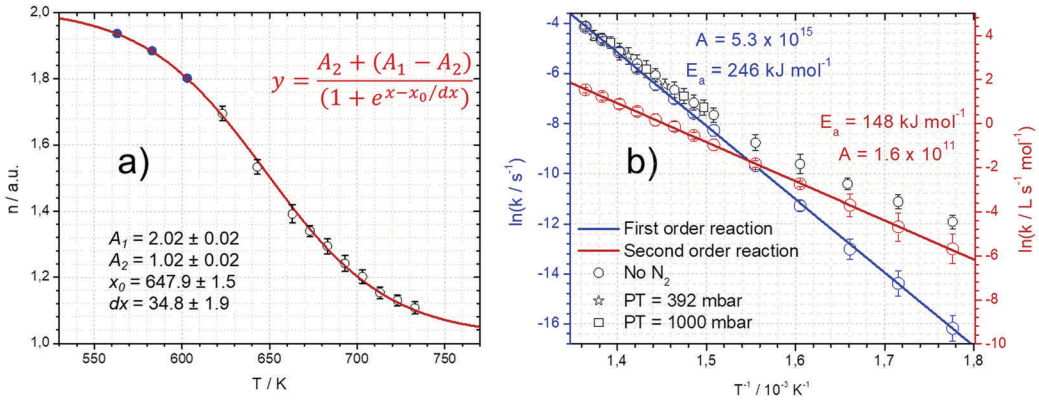

Fig. 3 (a) Reaction order (n) as a function of temperature (K). The experimental values were fitted with a sigmoidal function. The blue dots were taken from the fitted curve. (b) Logarithm of the rate constants as a function of T^{-1}. Red empty circles correspond to the second-order rate constants and blue empty circles correspond to the first-order rate constants obtained from the kinetic simulation. Black empty symbols correspond to the rate constants obtained using a direct first-order treatment (the values of the rate constants are presented in Table S1, ESI†).

The difference in the pre-exponential factor indicates that the transition state for the decomposition of $HC(O)OCH_3$ is tighter compared with $FC(O)OCH_3$.

Considering the pre-exponential factor for the bimolecular channel, the corresponding activation entropy is (-117.5 ± 0.8) J mol^{-1} K^{-1}. This is a clear indication that the reaction occurs by means of a much ordered transition state than at higher temperatures.

For the thermal decomposition of a related molecule, $ClC(O)OCH_3$, the informed value at 513 K is $k = (5.3 \pm 0.2) \times 10^{-6}$ s^{-1} considering the reaction as unimolecular decomposition.[39] The authors also found that, only ~63% follows the $ClC(O)OR \rightarrow RCl + CO_2$ path. In general, for the decomposition at temperatures lower than 540 K, authors postulate that heterogeneous reactions are involved. Nevertheless, in the present work it is evident that the bimolecular reaction (9) predominates at these temperatures for $FC(O)OCH_3$.

Table 1 presents the transition state's enthalpy, entropy and Gibbs free energies for the two channels (8) and (9) in the range of 563–733 K obtained from the kinetic analysis of the experimental Arrhenius plot. For a direct comparison, values for $HC(O)OCH_3$ and $ClC(O)OCH_3$ are also presented. The activation entropies for the unimolecular channels do not follow a clear tendency. In the case of the chlorinated molecule, the activation entropy informed is too low compared with the fluorinated one. This may be because the bimolecular channel was not considered for $ClC(O)OCH_3$. However, the values of activation enthalpy are very similar.

3.2. Thermal decomposition of $FC(O)OCH_2CH_3$

Thermal decomposition of $FC(O)OCH_2CH_3$ was also studied in the range of temperatures 433–623 K. Fig. 4 shows the reactant (10,1 ± 0.1 mbar) and the products of the thermal reaction after 300 seconds at 573 K. The main products found and the corresponding partial pressures after total decomposition were CO_2 (10.0 ± 0.1 mbar), CH_2CH_2 (9,3 ± 0.1 mbar) HF and CH_3CH_2F (undetermined pressures). Unlike the thermal decomposition of $FC(O)OCH_3$, no evidence of the bimolecular reaction products was observed (*i.e.* $CH_3CH_2OC(O)OCH_2CH_3$). Even more, when a mixture 1/1 of $FC(O)OCH_3$ and $FC(O)OCH_2CH_3$ reacts at 603 K,

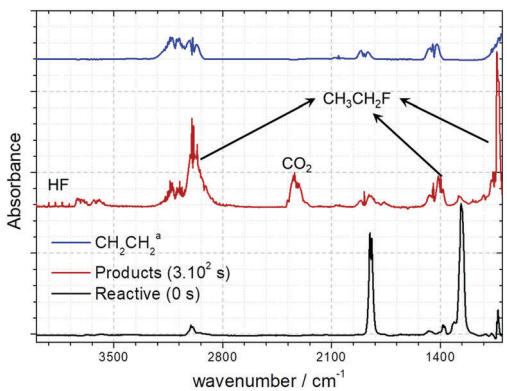

Fig. 4 IR spectra of $FC(O)OCH_2CH_3$ before (bottom) and after (middle) thermal exposure at 573 K. [a]Taken from the NIST database.

Table 1 Arrhenius parameters and thermodynamic values for the transition states for the thermal decomposition of $RC(O)OCH_3$. R = F at 698

	$FC(O)OCH_3$				
Thermodynamics	Bimolecular	Unimolecular	$FC(O)OCH_2CH_3$	$HC(O)OCH_3$[a]	$ClC(O)OCH_3$[b]
E_a (kJ mol^{-1})	148 ± 10	246 ± 10	169 ± 6	242	251
$\Delta H^{\#}$ (kJ mol^{-1})	142 ± 10	240 ± 10	164 ± 6	229	238
$\Delta S^{\#}$ (J mol^{-1} K^{-1})	−47 ± 6	+25 ± 6	−0.9 ± 3.7	−41.8	+0.6
$\Delta G^{\#}$ (kJ mol^{-1})	174 ± 15	222 ± 9	165 ± 6	288	238

[a] From ref. 12. [b] From ref. 16. $FC(O)OCH_2CH_3$ at 553 K.

the major products formed were $CH_3OC(O)OCH_3$, CH_3F, CO_2, HF and CH_2CH_2. No evidence of $CH_3CH_2OC(O)OCH_2CH_3$ nor $CH_3OC(O)OCH_2CH_3$ was observed.

Based on the products found, two concerted reaction paths are proposed.

$$FC(O)OCH_2CH_3 \rightarrow CO_2 + HF + CH_2CH_2 \quad (11)$$

$$FC(O)OCH_2CH_3 \rightarrow CO_2 + CH_3CH_2F \quad (12)$$

Okada *et al.* studied the thermal decomposition of CH_3CH_2F at 996–1137 K, and CH_2CH_2 and HF were the main products.[40]

$$CH_3CH_2F \rightarrow HF + CH_2CH_2 \quad (12')$$

In order to discard the step wise mechanism (reactions (12) and (12′)) in our system, some considerations about the kinetic parameters of reaction (12′) will be addressed. Matsugi *et al.* studied the thermal decomposition of fluoroethane by shock tube using infrared laser absorption detection of hydrogen fluoride[41] obtaining an expression for the rate constant of $3.3 \times 10^8\ (T/298)^{-14.94}\ \exp[-316.7\ \text{kJ mol}^{-1}/RT]$ [$\text{cm}^3\ \text{molecule}^{-1}\ \text{s}^{-1}$], which would give an approximate value of $k \approx 1 \times 10^{-40}\ \text{s}^{-1}$ at 573 K. This rate constant is too small to consider the formation of C_2H_4 and HF from CH_3CH_2F. Therefore, ethylene can be safely ascribed to the occurrence of reaction (11).

The kinetic parameters for the thermal decomposition of $FC(O)OCH_2CH_3$ were obtained from Fig. 5(a) and (b). The rate constants from the linear regressions of the first order plots are presented in Table S2 (ESI†). The Arrhenius parameters were obtained from Fig. 5(b), with the activation energy $E_a = (161 \pm 6)$ kJ mol^{-1} and the pre-exponential factor $A = (2.07 \pm 0.09) \times 10^{13}\ \text{s}^{-1}$. In this case, no deviation from linearity was observed from the Arrhenius fitting in the whole range of temperatures studied that include other points which are not shown in Fig. 5a. The value of activation energy is lower than the one found for $FC(O)OCH_3$.

The thermodynamic parameters for the transition state are shown in Table 1. The entropy is negative, unlike the case of $FC(O)OCH_3$. This is an indication of a more ordered transition state.

3.3. First principles calculations

Methyl fluoroformate. The $FC(O)OCH_3$ molecule presents two conformers, *cis* (*syn*, *Z*) and *trans* (*anti*, *E*) in agreement with the calculations made by Metcalfe *et al.* for the methyl formate.[42] The *cis* rotamer (O═C–O–C dihedral angle of 0°) is more stable by 13.9 kJ mol^{-1} than the *trans* rotamer (O═C–O–C dihedral angle of 180°), with an interconversion barrier $Z \rightleftharpoons E$ of 31 kJ mol^{-1}.

In order to obtain the heat of formation of methyl fluoroformate, we propose the isodesmic reaction:

$$FC(O)OCH_3 + CH_3C(O)CH_3 \rightarrow CH_3C(O)OCH_3 + FC(O)CH_3 \quad (13)$$

where the calculated reaction enthalpy at the G4 level of theory is -37.1 ± 0.6 kJ mol^{-1}. Together with the enthalpies of formation (ΔH_f) of $CH_3C(O)F = -445 \pm 2$,[43] $CH_3C(O)CH_3 = -217.9 \pm 0.7$,[44] and $CH_3C(O)OCH_3 = -413.5 \pm 1.2$,[45] this yields $\Delta H_f(298.15\ \text{K})$ of -603 ± 16 kJ mol^{-1} for the *cis*-conformer of methyl fluoroformate. As far as we are concerned, the experimental values of this enthalpy of formation have not been reported yet.

With the enthalpy just obtained and using the composite method G4, the bond dissociation energies were computed just to show that all single bond scission reactions in methyl fluoroformate have substantially higher barriers (>60 kJ mol^{-1}) than the transition states proposed as described in the next paragraph. The results are shown in Table 2, where we have also included ethyl fluoroformate.

Five unimolecular concerted channels were found for the gas-phase decomposition of methyl fluoroformate at different levels of theory. Fig. S2 (ESI†) shows the structure of these five transition states at the B3LYP level of theory, and Table 3 presents the barrier heights for each channel at the various levels of theory. These barrier heights are expressed relative to the *Z*-conformer of methyl fluoroformate and it is observed that all transition states overestimate the energy of the barrier when compared with the experimental result of 246 kJ mol^{-1}. A similar situation was observed for methyl formate as studied by Dooley *et al.*[46] *Ab initio* molecular orbital calculations performed by Francisco,[11] and calculations of the rate constants performed

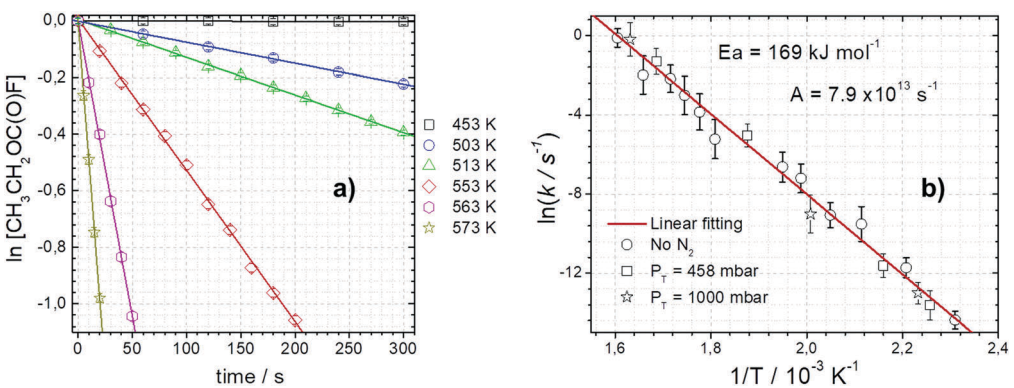

Fig. 5 (a) Logarithm of the concentration of $FC(O)OCH_2CH_3$ *vs.* time (in seconds), (b) Arrhenius plot of the logarithm of the rate constants as a function of T^{-1} at different total pressures.

 This journal is © the Owner Societies 2018

Table 2 Bond dissociation energies (kJ mol^{-1}) for $FC(O)OCH_3$ and $FC(O)OCH_2CH_3$ at different levels of theory

Bond	B3LYP[a]	MP2[a]	G4
D(F–C(O)OCH_3)	497.8	518.1	508.3
D(FC(O)–OCH_3)	420.1	469.6	429.6
D(FC(O)O–CH_3)	361.2	433.1	369.6
D(FC(O)OCH_2–H)	445.1	441.2	416.5
D(F–C(O)OCH_2H_3)	499.0	518.3	507.5
D(FC(O)–OCH_2H_3)	419.2	472.4	430.4
D(FC(O)O–CH_2CH_3)	362.8	445.3	379.2
D(FC(O)OCH_2–CH_3)	386.6	417.9	377.3
D(FC(O)OCH_2CH_2–H)	457.8	447.2	422.5

[a] Basis set: 6-31++G(d,p).

Table 3 Calculated transition state energies (kJ mol^{-1}) of the thermal decomposition of $FC(O)OCH_3$ at different levels of theory

	B3LYP		MP2		
	6-31++G(d,p)	6-311++G(3df,2pd)	6-31++G(d,p)	G2	G4
TS-1-M	260	263	288	271	276
TS-2-M	303	296	304	290	298
TS-3-M	379	376	401	375	379
TS-4-M	430	433	461	440	442
TS-5-M	523	525	451	—	423
TS-6-M	212	219	199	207	209

later by Metcalfe *et al.*,[42] overestimate the activation energy for the transition states of the three main channels, especially the one for the four center transition state that produces CH_4 and CO_2 (equivalent to the TS-1-M transition state in this work). They used a variety of methods and bases ranging from the simplest MP2 and B3LYP to multilevel methods like G3 and CBS-APNO to obtain consistent energies to describe the reaction mechanism, but they were all above the experimental energies found by Ren *et al.*[12] The activation energy calculated by Metcalfe for the formation of CO_2 and CH_4 was 348.3 ± 3.5 kJ mol^{-1} compared to the experimental energy of 241.8 kJ mol^{-1} found in shock tube/laser absorption studies of the direct high-temperature rate measurements for methyl formate decomposition. Even when the *ab initio* calculations overestimate the activation energy for these reaction channels, they can be used for the description of the reaction mechanism.

We have carried out B3LYP, MP2, G2MP2 and G4MP2 computations for all channels in order to give a qualitative description assisted by the *ab initio* method. The lowest energy path for the unimolecular channel corresponds to TS-1-M with all methods. Vibrational frequency calculations show that all the transition states are first-order saddle points, characterized by one imaginary frequency.

Even when this TS has the lowest activation energy, the methods overestimate the barrier height with an average of ~25 kJ mol^{-1}. An inspection of the values in Table 3 shows that the energy calculated with B3LYP and MP2 methods are very different than the values for G2 and G4 indicating that the electron correlation is important for this system. We consider 271 ± 20 kJ mol^{-1} to be the more appropriate theoretical value considering an overall error smaller than 10%. Within the error, this value agrees reasonably with the experimental value of 246 ± 10 kJ mol^{-1}. Intrinsic reaction coordinate calculations (IRC) at the B3LYP/6-311++G(3d,2p) level of theory shows that TS-1-M and TS-2-M connect the *E*-rotamer of $FC(O)OCH_3$, whereas TS-3-M, TS-4-M and TS-5-M connect the *Z* rotamer according to the following reactions:

$$E\text{-}FC(O)OCH_3 \rightarrow \text{TS-1-M} \rightarrow CH_3F + CO_2 \quad (14)$$

$$E\text{-}FC(O)OCH_3 \rightarrow \text{TS-2-M} \rightarrow HF + CH_2 + CO_2 \quad (15)$$

$$Z\text{-}FC(O)OCH_3 \rightarrow \text{TS-3-M} \rightarrow CHFO + CH_2O \quad (16)$$

$$Z\text{-}FC(O)OCH_3 \rightarrow \text{TS-4-M} \rightarrow FCOH + CH_2O \quad (17)$$

$$Z\text{-}FC(O)OCH_3 \rightarrow \text{TS-5-M} \rightarrow FCO + CH_3O \quad (18)$$

In addition, a sixth transition state was found for the bimolecular reaction, TS-6-M, where two molecules of methyl fluoroformate react to form a four center transition state. The final products of this channel found by IRC calculations are carbonyl fluoride and dimethyl carbonate:

$$2FC(O)OCH_3 \rightarrow \text{TS-6-M} \rightarrow CF_2O + CH_3OC(O)OCH_3 \quad (19)$$

Three structures were obtained for TS-6-M depending on the parent conformers *Z* + *E*; *E* + *E* and the dihedral $C^{1'}$–$O^{1'}$–$C^{2'}$–$O^{2'}$. The most stable structure comes from the reaction of *Z* + *E* with dihedral $C^{1'}$–$O^{1'}$–$C^{2'}$–$O^{2'}$ equal to −174.5°, which is more stable by 14.5 kJ mol^{-1} than the *E* + *E* structure. Taking into account the energy of this structure, the average calculated activation energy for this channel is 207 ± 15 kJ mol^{-1}. Once again, this value is very close to the Gn energies. The experimental activation energy informed in this work for the bimolecular channel is 148 ± 10 kJ mol^{-1} which is around 60 kJ mol^{-1} below the calculated one. It should be mentioned that the experimental value for E_a relies mainly on lower temperatures points (Fig. 3(b)). As the reaction is too slow under these conditions, the rate constants are less accurate. The calculated reaction path, TS-6-M, has the lowest activation energy of the six transition states found in this work, and would explain the appearance of $CH_3OC(O)OCH_3$ in our system. In addition, the calculated entropies for TS-1-M, $\Delta S^{\#}$ = +12.1 J K^{-1} mol^{-1}, and TS-6-M, $\Delta S^{\#}$ = −63.7 J K^{-1} mol^{-1}, are very similar to those of the experimental values. Scheme 1 summarizes the two most important channels found by *ab initio* calculation methods and the products of the reaction.

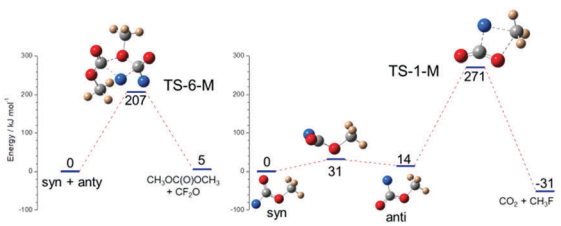

Scheme 1 Theoretical calculation of the most probable path for the $FC(O)OCH_3$ thermal decomposition. IRC calculations were performed for each transition state.

Ethyl fluoroformate. The dihedral C–C–O–C in the molecule $FC(O)OCH_2CH_3$ is 180.0, so this molecule presents only two conformers, *cis* (*syn*, *Z*) and *trans* (*anti*, *E*). In agreement with methyl fluoroformate, the *cis* rotamer (O=C–O–C dihedral angle of 0°) is more stable by 13.4 kJ mol^{-1} than the *trans* rotamer (O=C–O–C dihedral angle of 180°), with an interconversion barrier $Z \rightleftharpoons E$ of 44 kJ mol^{-1}, slightly higher than that for $FC(O)OCH_3$.

Similarly to the treatment for methyl fluoroformate, the enthalpy of formation, which is described for the first time, was calculated using the isodesmic reaction (20) with the reaction enthalpy $\Delta H_r = -35{,}6 \pm 0.6$ kJ mol^{-1} at the G4 level; in conjunction with $\Delta H_f(CH_3C(O)OCH_2CH_3) = -445.43 \pm 0.84$.[47] This yields ΔH_f(298.15 K) of -637 ± 17 kJ mol^{-1} for the ethyl fluoroformate.

$$FC(O)OCH_2CH_3 + CH_3C(O)CH_3 \rightarrow CH_3C(O)OCH_2CH_3 + FC(O)CH_3 \quad (20)$$

Bond dissociation energies for this molecule are ~120 kJ higher than the transition states proposed so that all unimolecular scission were therefore discarded (Table 2).

Six TS structures similar to the $FC(O)OCH_3$ system were found for the ethyl fluoroformate. Fig. S3 (ESI†) shows the structures of all TSs and Table 4 presents the activation energies for each one. Again, the calculations overestimate the energy of the barriers by ~36 kJ mol^{-1}; therefore their comparison should be taken carefully as an indication of their relative positions in the PES but not as quantitative values.

From the transition states found for the unimolecular decomposition, and the IRC calculations, we can postulate the reactions:

$$FC(O)OCH_2CH_3 \rightarrow \text{TS-1-}E \rightarrow CH_3CH_2F + CO_2 \quad (21)$$

$$FC(O)OCH_2CH_3 \rightarrow \text{TS-2-}E \rightarrow HF + CH_2CH_2 + CO_2 \quad (22)$$

$$FC(O)OCH_2CH_3 \rightarrow \text{TS-3-}E \rightarrow CH_3C(O)H + FCHO \quad (23)$$

$$FC(O)OCH_2CH_3 \rightarrow \text{TS-4-}E \rightarrow CH_3C(O)H + FCOH \quad (24)$$

$$FC(O)OCH_2CH_3 \rightarrow \text{TS-5-}E \rightarrow FCO + CH_3CH_2O \quad (25)$$

$$2FC(O)OCH_2CH_3 \rightarrow \text{TS-6-}E \rightarrow CF_2O + (CH_3CH_2O)_2CO \quad (26)$$

Table 4 Calculated transition state energies (kJ mol^{-1}) of the thermal decomposition of $FC(O)OCH_2CH_3$ at different levels of theory

	B3LYP		MP2		
	6-31++G(d,p)	6-311++G(3df,2pd)	6-31++G(d,p)	G2	G4
TS-1-*E*	232	234	245	235	239
TS-2-*E*	199	200	214	207	208
TS-3-*E*	342	342	353	334	334
TS-4-*E*	426	429	436	427	424
TS-5-*E*	527	529	435	412	422
TS-6-*E*	242	248	240[a]	—	—

[a] Optimization performed with MP2/3-21G; energy calculation performed with 6-31++G(d,p).

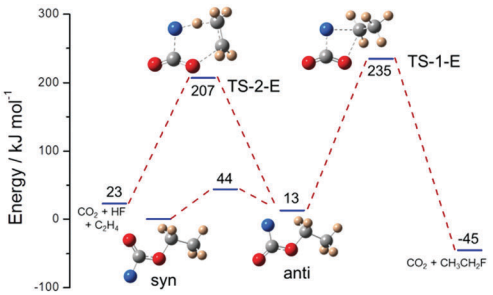

Scheme 2 Theoretical calculation of the most probable path for $FC(O)OCH_2CH_3$ thermal decomposition. IRC calculations were performed for each transition state.

It is interesting to note that the transition state for the bimolecular reaction (TS-6-*E*) do not have the lowest activation energy. The two more probable channels, based on the TS energies, are (21) and (22), which agree with the experimental products found. From the experimental ratio of concentrations (pressures) $[CH_2CH_2]/[CO_2]_{total}$ we can assume that 94 ± 2% of the reaction undergoes channel (22) and therefore only 6 ± 4% follows channel (21).

Scheme 2 summarizes the mechanism proposed indicating the main structures of the PES. Both transition states proceed from the *E*-conformer. TS-1-*E* is a four-center transition state, while TS-2-*E* is a six-center structure. The stability of six-center structures over the four-center transition state is well known for this kind of processes.[48,49] As stated before, the major path in this case (channel (22)) is a unimolecular concerted reaction. This could explain the fact that no deviation in the Arrhenius plot was observed for the thermal reaction of $FC(O)OCH_2CH_3$. The calculated entropy for TS-2-*E* is -6 J mol^{-1} K^{-1} compared with the experimental value of -1 ± 4 J mol^{-1} K^{-1}, are similar within the error.

Conclusions

The thermal decomposition of the two smaller members of the family of fluoroformates was investigated using FTIR spectroscopy and first principles calculations.

In the case of $FC(O)OCH_3$ the experimental data indicate two different channels. At temperatures higher than 660 K, reaction (8) is the main channel and the products are CH_3F and CO_2. There is no indication of formation of radicals, so the mechanism proposed is an elementary reaction with a four center TS. At lower temperatures the decomposition is dominated by the bimolecular reaction (9), which produces $CH_3OC(O)OCH_3 + CF_2O$. Both channels have been explored by kinetics simulations and first principles calculations. This second channel has not been informed for the decomposition of methyl formates.

The thermal decomposition of ethyl fluoroformate proceeds mainly through reaction (22) which produces HF, C_2H_2 and CO_2. All the experimental data points lie on a straight line on the Arrhenius plot in the temperature range studied. The mechanism proposed for this channel involves a six center TS. Nevertheless, as

 This journal is © the Owner Societies 2018

CH_3CH_2F was detected as a minor product, reaction (21) has to be considered as the secondary channel.

Conflicts of interest

There are no conflicts to declare.

Acknowledgements

Financial support from Consejo Nacional de Investigaciones Científicas y Técnicas (CONICET), FONCyT, and SECyT-UNC is gratefully acknowledged. Ms. M. F. Palmero is grateful acknowledged for language assistance.

References

1 M. A. Burgos Paci and G. A. Argüello, Kinetics of the reaction between CF_2O and CH_3OH, *Proc. Env. Simul. Chambers.*, 2006, 207–212.
2 M. Berasategui, M. A. Burgos Paci and G. A. Argüello, Isolation and characterization of $CH_3OC(O)OOC(O)F$ from the reaction CH_3OH + FC(O)OOC(O)F, *Z. Anorg. Allg. Chem.*, 2012, **638**, 547–552.
3 S. M. Japar, T. J. Wallington, J. F. O. Richert and J. C. Ball, The atmospheric chemistry of oxygenated fuel additives: *t*-butyl alcohol, dimethyl ether, and methyl *t*-butyl ether, *Int. J. Chem. Kinet.*, 1990, **22**, 1257–1269.
4 M. E. Jenkin, G. D. Hayman, T. J. Wallington, M. D. Harley, J. C. Ball, O. J. Nielsen and T. Ellerman, Kinetic and mechanistic study of the self-reaction of methoxymethylperoxy radicals at room temperature, *J. Phys. Chem.*, 1993, **97**, 11712–11723.
5 J. Wenger, E. Porter, E. Collins, J. Treacy and H. Sidebottom., Mechanisms for the chlorine atom initiated oxidation of dimethoxymethane and 1,2-dimethoxyethane in the presence of NO_x, *Chemosphere*, 1999, **38**, 1197–1204.
6 I. Liu, N. W. Cant, J. H. Bromly, F. J. Barnes, P. F. Nelson and B. S. Haynes, Formate species in the low-temperature oxidation of dimethyl ether, *Chemosphere*, 2001, **42**, 583–589.
7 H. von Blottnitz and M. A. Curran, A review of assessments conducted on bio-ethanol as a transportation fuel from a net energy, greenhouse gas, and environmental life cycle perspective, *J. Cleaner Prod.*, 2007, **15**, 607–619.
8 E. W. Steacie, The kinetics of the heterogeneous thermal decomposition of methyl formate, *Proc. R. Soc. London*, 1930, **127**, 314–330.
9 D. V. S. Jain and B. S. Murwaha, Kinetics of thermal decomposition of methyl formate in gas phase, *Indian J. Chem.*, 1969, **7**, 901–902.
10 C. P. Davis, PhD thesis, Graduate School of Science, University of Mississippi, Oxford, Mississippi, 1983.
11 J. S. Francisco, Mechanistic study of the gas-phase decomposition of methyl formate, *J. Am. Chem. Soc.*, 2003, **125**, 10475–10480.
12 W. Ren, K. Y. Lam, S. H. Pyun, A. Farooq, D. F. Davidson and R. K. Hanson, Shock tube/laser absorption studies of the decomposition of methyl formate, *Proc. Combust. Inst.*, 2013, **34**, 453–461.
13 H. C. Ramsperger and G. Waddington., The kinetics of the thermal decomposition of trichloromethyl chloroformate, *J. Am. Chem. Soc.*, 1933, **55**, 214–220.
14 W. Hentschel, Übergefrorene Ameisensäuremethyläther und verwandte Körper, *J. Prakt. Chem.*, 1887, **2**, 36.
15 V. Grignard, G. Rivat and E. Urbain, Preparation of chloromethyl carbonate, *Ann. Chim.*, 1920, **13**, 229–265.
16 R. L. Johnson and V. R. Stimson., The thermal decomposition of methyl chloroformate, *Aust. J. Chem.*, 1977, **30**, 1917–1920.
17 S. Nakanishi, T. C. Myers and E. V. Jensen., Synthesis of alkyl fluorides from alcohols *via* fluoroformate esters, *J. Am. Chem. Soc.*, 1955, **77**, 3099–3100.
18 E. P. Hunter and S. G. Lias, Evaluated gas phase basicities and proton affinities of molecules: an update, *J. Phys. Chem. Ref. Data*, 1998, **27**, 413–656.
19 J. M. Desmarchelier, Ethyl formate and formic acid: occurrence and environmental fate, *Postharvest News Inf.*, 1999, **10**, 7–12.
20 T. Hiroyasu, C. Shibanuma, H. Ishii, R. Yamada and C. Nakamura, Studies on the sugars organic acids and volatile compounds in grape-berries, *Tech. Bull. Fac. Hortic., Chiba Univ.*, 1972, **20**, 51–60.
21 T. Simpson, V. Bikoba and E. J. Mitcham, Effects of ethyl formate on fruit quality and target pest mortality for harvested strawberries, *Postharvest Biol. Technol.*, 2004, **34**, 313–319.
22 T. Simpson, V. Bikoba, C. Tipping and E. J. Mitcham., Ethyl formate as a postharvest fumigant for selected pest of table grapes, *J. Econ. Entomol.*, 2007, **100**, 1084–1090.
23 L. E. Vincent and D. L. Lindgren, Hydrogen phosphide and ethyl formate: fumigation of insects infesting dates and other dried fruits, *J. Econ. Entomol.*, 1972, **65**, 1667–1669.
24 Toxicological and regulatory information supporting the registration of VAPORMATE™ as a grain fumigant for farm storages. *Australian Postharvest Technical Conference*, ed. V. S. Haritos, K. A. Damcevski, G. Dojchinov, E. J. Wright, M. C. Webb, E. Highley, CSIRO Stored Grain Research Laboratory, Canberra, 2003, pp. 193–198.
25 J. Eberhard, C. Müller, D. W. Stocker and J. A. Kerr, The photo-oxidation of diethyl ether in smog chamber experiments simulating tropospheric conditions. Products studies and proposed mechanism, *Int. J. Chem. Kinet.*, 1993, **25**, 639–649.
26 T. J. Wallington and S. M. Japar, Atmospheric chemistry of diethyl ether and ethyl *tert*-butyl ether, *Environ. Sci. Technol.*, 1991, **25**, 410–415.
27 A. Belloche, R. T. Garrod, H. S. P. Müller, K. M. Menten, C. Comito and P. Schilke., Increased complexity in interstellar chemistry: detection and chemical modeling of ethyl formate and *n*-propyl cyanide in Sagittarius B2(N), *Astron. Astrophys.*, 2009, **499**, 215–232.

28 Y.-C. Chou, A theoretical investigation of the decomposition reactions of ethyl formate in the S_0 state, *J. Chin. Chem. Soc.*, 2012, **59**, 1528–1535.

29 Y.-C. Chou, A theoretical investigation of the decomposition reactions of ethyl formate in the S_1 and T_1 states, *J. Chin. Chem. Soc.*, 2013, **60**, 608–617.

30 A. T. Blades., The kinetics of the pyrolysis of ethyl and isopropyl formates and acetates, *Can. J. Chem.*, 1954, **32**, 366–372.

31 O. N. Ventura and M. Kieninger., The FO_2 radical: a new success of density functional theory, *Chem. Phys. Lett.*, 1995, **245**, 488–497.

32 K. Raghavachari, B. Zhang, J. A. Pople, B. G. Johnson and P. M. W. Gill, Isomers of C_{24}. Density functional studies including gradient corrections, *Chem. Phys. Lett.*, 1994, **220**, 385–390.

33 B. G. Johnson, C. A. Gonzalez, P. M. W. Gill and J. A. Pople, A density functional study of the simplest hydrogen abstraction reaction. Effect of self-interaction correction, *Chem. Phys. Lett.*, 1994, **221**, 100–108.

34 C. Lee, W. Yang and R. G. Parr, Development of the Colle-Salvetti correlation-energy formula into a functional of the electron density, *Phys. Rev. B: Condens. Matter Mater. Phys.*, 1988, **37**, 785–789.

35 M. J. Frisch, G. W. Trucks, H. B. Schlegel, G. E. Scuseria, M. A. Robb, J. R. Cheeseman, G. Scalmani, V. Barone, B. Mennucci, G. A. Petersson, H. Nakatsuji, M. Caricato, X. Li, H. P. Hratchian, A. F. Izmaylov, J. Bloino, G. Zheng, J. L. Sonnenberg, M. Hada, M. Ehara, K. Toyota, R. Fukuda, J. Hasegawa, M. Ishida, T. Nakajima, Y. Honda, O. Kitao, H. Nakai, T. Vreven, J. A. Montgomery, Jr., J. E. Peralta, F. Ogliaro, M. Bearpark, J. J. Heyd, E. Brothers, K. N. Kudin, V. N. Staroverov, R. Kobayashi, J. Normand, K. Raghavachari, A. Rendell, J. C. Burant, S. S. Iyengar, J. Tomasi, M. Cossi, N. Rega, J. M. Millam, M. Klene, J. E. Knox, J. B. Cross, V. Bakken, C. Adamo, J. Jaramillo, R. Gomperts, R. E. Stratmann, O. Yazyev, A. J. Austin, R. Cammi, C. Pomelli, J. W. Ochterski, R. L. Martin, K. Morokuma, V. G. Zakrzewski, G. A. Voth, P. Salvador, J. J. Dannenberg, S. Dapprich, A. D. Daniels, O. Farkas, J. B. Foresman, J. V. Ortiz, J. Cioslowski and D. J. Fox, *Gaussian 09, Revision A.02*, Gaussian, Inc., Wallingford, CT, 2009.

36 A. J. Pepino, W. J. Peláez and G. A. Argüello, From new simple aliphatic to aromatic heterocycles built from 2-chloroethylisocyanate, *J. Anal. Appl. Pyrolysis*, 2014, **105**, 49–54.

37 S. L. Peukert, R. Sivaramakrishnan and J. V. Michael., High temperature shock tube studies on the thermal decomposition of O_3 and the reaction of dimethyl carbonate with O-atoms, *J. Phys. Chem. A*, 2013, **117**, 3729–3738.

38 J. C. Kintecus, *Ianni. version 5.5*, 2015.

39 E. S. Lewis and W. C. Herndon., The decomposition of gaseous chloroformates. I. The rates of simple alkyl compounds, *J. Am. Chem. Soc.*, 1961, **83**, 1955–1958.

40 K. Okada, E. Tschuikow-Roux and P. J. Evans, Single-pulse shock-tube study of the thermal decomposition of ethyl fluoride and *n*-propyl chloride, *J. Phys. Chem.*, 1980, **84**, 467–471.

41 A. Matsugi and H. Shiina., Shock tube study on the thermal decomposition of fluoroethane using infrared laser absorption detection of hydrogen fluoride, *J. Phys. Chem. A*, 2014, **118**, 6832–6837.

42 W. K. Metcalfe, J. M. Simmie and H. J. Curran, Ab initio chemical kinetics of methyl formate decomposition: the simplest model biodiesel, *J. Phys. Chem. A*, 2010, **114**, 5478–5484.

43 H. O. Pritchard and H. A. Skinner, The heat of hydrolysis of acetyl fluoride, *J. Chem. Soc.*, 1950, 1099.

44 K. B. Wiberg, L. S. Crocker and K. M. Morgan., Thermochemical studies of carbonyl compounds. **5**. Enthalpies of reduction of carbonyl groups, *J. Am. Chem. Soc.*, 1991, **113**, 3447–3450.

45 S. P. Verevkin, H.-D. Beckhaus, R. S. Belen'kaja, K. Rakus and C. Ruchardt., Geminal substituent effects. Part 9 *. Standard formation enthalpies and stress-free increments of branched esters and ethers, *Thermochim. Acta*, 1996, **279**, 47–64.

46 S. Dooley, M. P. Burke, M. Chaos, Y. Stein, F. L. Dryer, V. P. Zhukov, O. Finch, J. M. Simmie and H. J. Curran, Methyl formate oxidation: speciation data, laminar burning velocities, ignition delay times, and a validated chemical kinetic model, *Int. J. Chem. Kinet.*, 2010, **42**, 527–549.

47 K. B. Wiberg, L. S. Crocker and K. M. Morgan, Thermochemical studies of carbonyl compounds. **5**. Enthalpies of reduction of carbonyl groups, *J. Am. Chem. Soc.*, 1991, **113**, 3447–3450.

48 Y. Maroni-Barnaud, P. Maroni and A. M. Fualdes, I-4 addition of α-branched alkyl magnesium halides to aromatic alonones: synthesis of a series of ketones, *Comptes Rendus*, 1962, **254**, 2360–2362.

49 R. B. Mane and G. S. Krishna Rao., Studies in terpenoids. Part XXIII. An approach to the 1-aryl-1,2,2-trimethylcyclopentane skeleton by intramolecular ketocarbene insertion. Synthesis of β-cuparenone, *J. Chem. Soc., Perkin Trans. 1*, 1973, 1806–1808.

 This journal is © the Owner Societies 2018